Thermally Activated Delayed Fluorescence of Dibenzophenazine-Cored Phenazaborines in Solid State: Anion Modulation of Photophysics

Jaijanarthanan Lingagouder,[a] Nae Aota,[b] Riku Nakagawa,[b] Beata Luszczynska,[a] Satoshi Minakata,[b] Leonardo Evaristo de Sousa,[c] Piotr de Silva,[c] Przemyslaw Data,*[a] and Youhei Takeda*[b]*

[a] Department of Molecular Physics, Faculty of Chemistry, Lodz University of Technology, 90-543 Lodz, Poland.

[b] Department of Applied Chemistry, Graduate School of Engineering, Osaka University, Suita, Osaka 565-0871, Japan.

[c] Department of Energy Conversion and Storage, Technical University of Denmark, Anker Engelunds Vej 301, 2800 Kongens Lyngby, Denmark.

KEYWORDS. Thermally activated delayed fluorescence, boron, organic light-emitting diodes, donor-acceptor system, charge transfer.

ABSTRACT. The relentless pursuit of high-performance organic light-emitting diodes (OLEDs) necessitates the exploration of novel materials with efficient light emission. Herein, we report donor–acceptor–donor (D–A–D) compounds, incorporating dibenzo[*a,j*]phenazine (DBPHZ) as the acceptor (A) and phenazaborine (PAzB) derivatives as the donors (D), embedded in various hosts, and investigate their impact on emission mechanisms. This study examines the effect of strategic fluorination of the trivalent boron center on the performance of the D–A–D compounds as solid-state emitters. The incorporation of fluoride into the D–A–D compounds within the matrix films resulted in a red shift in photoluminescence (PL) emission. Additionally, we evaluated the influence of fluoride addition on the delayed emission characteristics of the D–A–D containing films. This solid-state modulation technique demonstrated potential applicability to OLEDs. Quantum chemical calculations elucidated how fluoride incorporation alters the photophysical properties of the compounds by modifying the electronic characteristics of the excited states.

INTRODUCTION.

Thermally activated delayed fluorescence (TADF) is a fundamental photophysical phenomenon characterized by exciton dynamics involving reverse intersystem crossing (rISC) from an energetically proximate triplet excited state (T_n) to a singlet excited state (S_1), followed by radiative decay from S_1, resulting in delayed emission on the microsecond timescale.[1] To facilitate the inherently spin-forbidden rISC process and enhance TADF, a small singlet-triplet energy gap (ΔE_{ST} < ca. 0.3 eV) and substantial spin-orbit coupling (SOC) are essential.[2,3]

TADF-active organic compounds, which can efficiently harvest both singlet and triplet excitons to produce light without the incorporation of heavy atom elements, have emerged over the past decade as the third generation of emissive materials for high-efficiency organic light-emitting diodes (OLEDs).[4–6] Recently, TADF-active organic compounds have expanded their utility to diverse applications such as oxygen sensors,[7] time-resolved bio-imaging probes,[8] and scintillators.[9] Moreover, integrating TADF function with other photonic properties within a single molecular scaffold paves the way for novel applications beyond traditional optoelectronic and biological technologies.[10] Consequently, the development of new TADF-active organic compounds and the exploration of their functional aspects is of fundamental importance.

Triarylborane (TAB) compounds have garnered significant attention as photo- and electro-active functional organic materials, owing to their Lewis acidity, which stems from a vacant p-orbital, and their expanded π-electron systems.[11,12] Specifically, fluoride sensors based on the TAB scaffold have been extensively studied, leveraging the Lewis acidity of the trivalent boron center and the thermodynamically favorable formation of strong B–F bonds.[13] However, most reported TAB-based fluoride sensors exhibit colorimetric and fluorometric blue-shifts or emission turn-off, due to molecular design principles that disrupt π-conjugation[14,15] or suppress intramolecular charge-transfer (CT).[16]

Recently, we successfully developed TAB compounds (**1-Mes** and **1-Tipp**, Figure 1a) that display colorimetric and fluorometric red-shifts upon fluoride coordination.[17] These TAB compounds consist of two phenazaborine (PAzB) units orthogonally connected to a dibenzo[*a,j*]phenazine (DBPHZ) core.[18] The ambipolar structure of PAzB allows it to function both as a Lewis acid and an electron donor,[17] facilitating a red-shift in absorption and PL upon

fluoride coordination to the trivalent boron center by enhancing ICT from PAzB to the more electron-deficient DBPHZ unit (Figure 1b).

Concerning the relationship between PAzB structure and TADF, PAzBs have emerged as multi-resonance TADF emitters, due to their bipolar electronic configuration.[19–21] In our previous study, we primarily focused on anion-responsive photophysical changes in diluted solutions, preliminarily identifying emission red-shifts through ICT enhancement in a polymer matrix via the formation of fluoroborates. Given that compounds **1-Mes** and **1-Tipp** possess a DBPHZ-cored D–A–D structure, which is promising for manifesting TADF functions,[22–24] we hypothesized that these compounds could exhibit TADF in condensed states such as polymer-doped films.

Herein, we disclose the investigation of the TADF behavior of **1-Mes** and **1-Tipp** in matrix films, both in the absence and presence of fluoride. Furthermore, OLED devices utilizing these compounds as emitter were fabricated, and their performances were assessed to elucidate the effect of fluoride addition on TADF properties. Theoretical calculations revealed that fluorination of the boron center of the compounds induces significant changes in their photophysical mechanisms, resulting in double emission (fluorescence and RTP) that leads to delayed emission. This phenomenon is ascribed to the alternation in the electronic character of the lower-lying singlet and triplet states, which acquire a much stronger CT character.

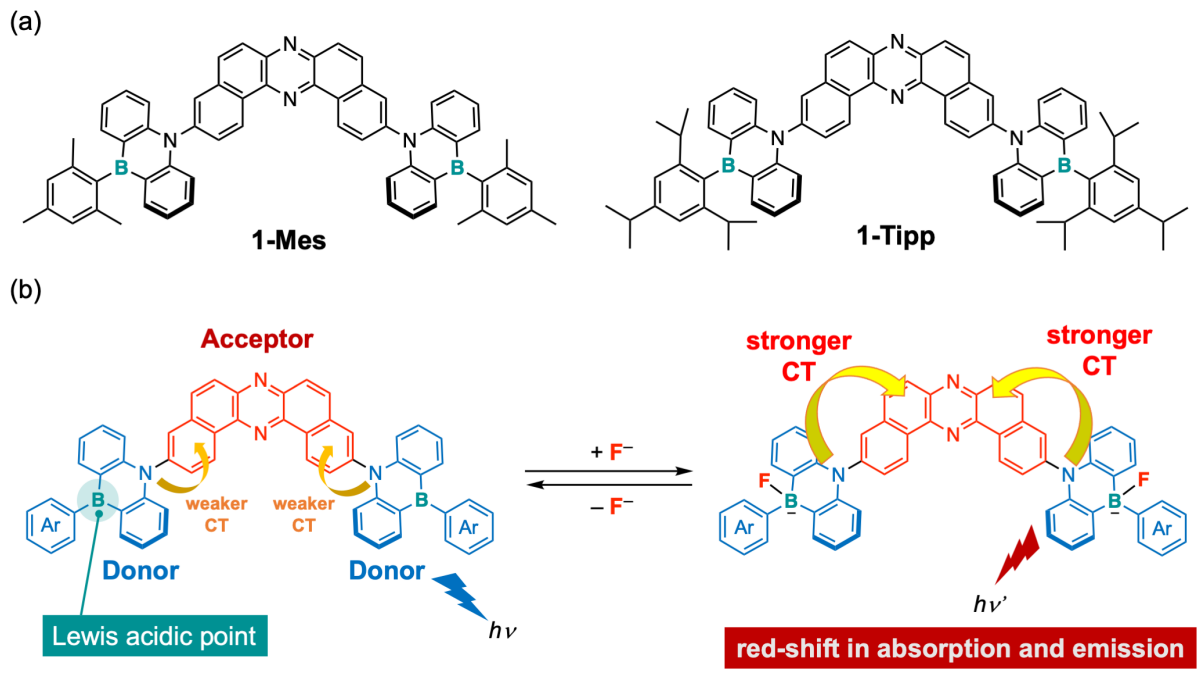

Figure 1. (a) Chemical structure of **1-Mes** and **1-Tipp**. (b) Illustrative principle of colorimetric and fluorometric red-shift of DBPHZ-cored phenazaborine compounds.

EXPERIMENTAL PROCEDURES

Materials. The compounds **1-Mes** and **1-Tipp** investigated in this study were prepared and characterized in our previous publication,[17] and the same batches of these compounds were used in the present research.

Photophysical analysis. The emissive properties of the entire set of dyes were analyzed in non-polar Zeonex® and polar 4,4'-bis(*N*-carbazolyl)-1,1'-biphenyl (CBP) host matrices.

Films containing **1-Mes** and **1-Tipp** in the Zeonex® matrix were prepared using toluene solvents, where the compounds and Zeonex® were initially dissolved. Subsequently, the

solutions were mixed to obtain a specific concentration of the compound in the Zeonex® matrix (e.g., 1%), then then spin-coated at 2000 RPM onto sapphire substrates to form uniform layers. Samples in the CBP matrix were prepared in a chloroform/chlorobenzene (95:5 *v*/*v*) solution and spin-coated at 3000 RPM onto sapphire substrates to form uniform layers.

1-Mes+F and **1-Tipp+F** in the Zeonex® matrix were prepared using toluene/THF solvents. Initially, the compound (**1-Mes** and **1-Tipp**) dissolved in toluene was mixed with a 1 M tetra(*n*-butyl)ammonium fluoride (TBAF) THF solution, while Zeonex® was dissolved in toluene to obtain a concentration of 200 mg/mL. In the next step, the solutions were combined to obtain a 1% concentration of the emitter in the Zeonex® matrix. The resulting mixture was then spin-coated at 2000 RPM onto sapphire substrates to form uniform layers. Samples in the CBP matrix were prepared similarly using toluene to obtain a 10% concentration of the emitter, and were spin-coated at 3000 RPM onto sapphire substrates to form uniform layers.

Phosphorescence, prompt fluorescence (PF), and delayed fluorescence (DF) spectra and decays were recorded using nanosecond-gated luminescence and lifetime measurements, ranging from 400 ps to 1 s. These measurements were performed with the third harmonics of a high-energy pulsed DPSS laser emitting at 355 nm (Q-Spark A50-TH-RE). Emission was focused onto a spectrograph and detected using a sensitive gated iCCD camera (Stanford Computer Optics) with sub-nanosecond resolution. PF/DF time-resolved measurements were conducted by exponentially increasing the gate and integration times. Temperature-dependent experiments were carried out using a helium cryostat (Janis Research) under vacuum conditions.

Fabrication of OLED Devices and Evaluation of the Performances. The solution-processed OLEDs were fabricated using the spin-coating method with a 10% (*w*/*w*) concentration of the

emitters in the CBP host. The device configuration was as follows: ITO/poly(3,4-ethylenedioxythiophene):poly(styrenesulfonate) (PEDOT:PSS-Clevios) (40 nm)/ emitter + CBP (30 nm)/TPBi [2,2',2"-(1,3,5-benzinetriyl)-tris(1-phenyl-1-*H*-benzimidazole)] (50 nm)/LiF (1 nm)/Al (100 nm), with the last three layers deposited by evaporation. PEDOT:PSS was spin-coated after filtering at 3000 RPM for 45 s, resulting in 40 nm layers, and then annealed at 120 °C for 15 minutes. Emitters **1-Mes** and **1-Tipp** were spin-coated from a chloroform/chlorobenzene (95:5 *v*/*v*) solution at 3000 RPM for 45 s without annealing. Emitters **1-Mes+F** + **1-Tipp+F** were spin-coated from a toluene/THF (50:50, *v*/*v*) solution under the same conditions. The samples were then transferred to a vacuum chamber for the deposition of the remaining layers. All small molecules and cathode layers were thermally evaporated in a Kurt J. Lesker Spectros evaporation system under a pressure of 10^{-7} mbar without breaking the vacuum. Pixel sizes were 4 mm^2, 8 mm^2, and 16 mm^2. Each emitting layer was formed by multiple depositions of the TADF emitter, assistant dopant, and host at specific rates to obtain the desired material composition. The device characteristics were recorded using a 6-inch integrating sphere (Labsphere) inside a glovebox connected to a Source Meter Unit and an Ocean Optics USB4000 spectrometer.

Quantum Chemical Calculations. Calculations were performed with density functional theory (DFT) using a non-empirically tuned LC-ωPBE functional and the 6-31G(d,p) basis set. Excited state calculations made use of the Tamm-Dancoff approximation.[25] Perturbative state-specific solvation corrections are applied to account for dielectric effects on the energies.[26] Optical spectra and photophysical transition rate constants were computed using the nuclear ensemble method as implemented in the NEMO software,[27,28] interfaced with QChem 6.0.[29] Ensembles of

500 geometries at 300 K were used in all cases. The calculated rate constants were used in a kinetic model[27] to simulate the populations of excited states and emission intensity decay profiles.

RESULTS AND DISCUSSION

The photophysical properties of these samples were thoroughly characterized using PL spectroscopy to determine emission wavelengths and analyze the singlet and triplet excited states. Time-resolved spectroscopy was employed to investigate delayed fluorescence mechanisms, including RTP and triplet-triplet annihilation (TTA). The emission spectra of the emitters revealed a pronounced bathochromic shift (red-shift) upon the addition of fluoride to both **1-Mes** and **1-Tipp** in both Zeonex® and CBP hosts (Figure 2 and 3). This shift indicates a decrease in the energy of the S_1 state due to the stabilization of the CT excited state by the coordination of fluoride to the trivalent boron center. This observations are consistent with theoretical predictions for fluoroborate organic molecules (*vide infra*).

Emission Properties in Zeonex Matrix

For neutral-state emitters in the Zeonex® matrix, the emission wavelengths maxima were recorded at 449 nm for **1-Mes** and 445 nm for **1-Tipp**, corresponding to the lowest singlet excited states with CT character (^{1}CT), showing no significant impact from the aryl substituent (Mes vs. Tipp) on the donor (Figure 2a and 3a). The lowest triplet excited states for both samples were observed at 2.31 eV, indicating no significant impact from the donor moiety and suggesting that the triplet state is localized (^{3}LE) on the DBPHZ acceptor unit (Figure 2a and 3a). The moderately large singlet-triplet gap for both samples resulted in mixed TTA and RTP emissions (Figure 2a, 3a. and Figure S1). Quantum chemical calculations of **1-Mes** in Zeonex® (ε=2.35,

n_r=1.53) predict fluorescence from a localized S_1 state with a peak at approximately 2.68 eV (463 nm) and a low emission rate (k_f = 8 ± 1×10^6 s^{-1}), which contrasts with the experimental observation of fluorescence in the ns time scale (Table 1). However, in the S_2 state, the ensemble has a mixed CT/LE character with an emission peak at 2.92 eV (425 nm) and a larger fluorescence rate (k_f = 1.52 ± 0.09×10^8 s^{-1}), aligning more closely with experimental results (Figure S2). The overlap of both emission spectra suggests a reordering of states due to stronger stabilization of the CT states in polar environments (Figure S3), effectively making it lower in energy than the calculated S_1. The T_1 emission peak of **1-Mes** is predicted at 1.98 eV (626 nm) and is localized on the acceptor unit (Figure S4). For **1-Mes**, rISC processes to S_1 and S_2 in Zeonex® have average gaps of 0.291 eV and 0.480 eV, respectively, with average SOC of 0.107 meV and 0.002 meV. This combination results in very low rISC rates, making phosphorescence the more efficient radiative deactivation mechanism for triplets in **1-Mes** (k_p= 1.3 ± 0.1×10^2 s^{-1}).

Formation of fluoroborate of **1-Mes** and **1-Tipp** resulted in significant red shifts in the emission wavelengths in the Zeonex® host, with **1-Mes+F** emitting at 596 nm and **1-Tipp+F** at 565 nm. This was accompanied by a decrease in the ^{1}CT energy of the singlet excited state (Figure 2e and 3e). Additionally, the lowest triplet excited states were observed to drop to 1.87 eV for **1-Mes+F** and 1.95 eV for **1-Tipp+F** (Figure 2e and 3e). This reduction in energy was accompanied by a narrowing of the singlet-triplet energy gaps to 0.21 eV for **1-Mes+F** and 0.23 eV for **1-Tipp+F**, facilitating the rISC process with TADF emission and additional RTP emissions at longer delay times (Figure 2e, 3e, and Table 1). These observations are consistent with theoretical calculations, which show that for **1-Mes-2F** in Zeonex®, S_1 emission has clear CT character and peaks at 1.85 eV (671 nm) with less efficient fluorescence (k_f = 8.1 ± 0.8×10^6 s^{-1}) compared to **1-Mes** (Figure S3). Calculations also predict a lowering of the T_1 state, with the

emission peak shifting to 1.60 eV (773 nm) (Figure S4). This new arrangement results in a much more efficient rISC process (k_{rISC} = 7 ± 5×10^8 s^{-1}), with a near-zero average gap and significantly stronger average SOC (1.149 meV) due to the formation of fluoroborate. The reduction in the singlet-triplet gap also leads to high ISC rates (k_{ISC} = 1.8 ± 0.2×10^8 s^{-1}).

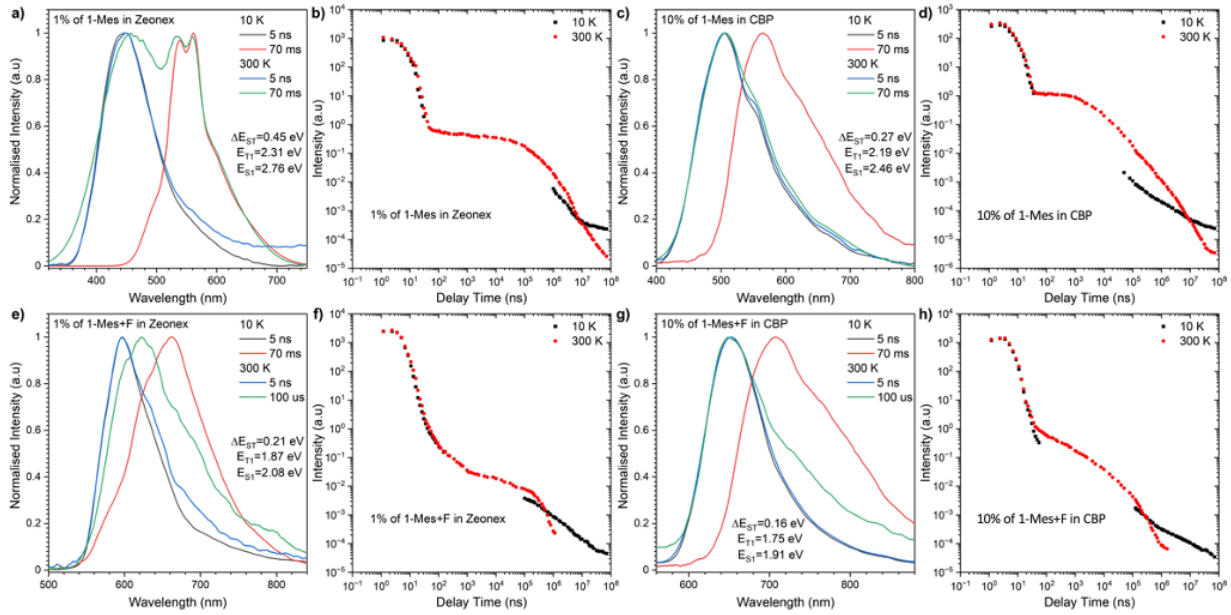

Figure 2. Time-resolved PL spectra (a, c, e, and g) and decay profiles (intensity vs. delay time) (b, d, f, h) of **1-Mes** and **1-Mes+F** in Zeonex® and CBP. The energies correspond to the maximum emission peaks.

Emission Properties in CBP Matrix

In the CBP matrix, the emission properties exhibited distinct characteristics. For neutral emitters **1-Mes** and **1-Tipp**, the emission wavelengths were recorded at 504 nm and 477 nm, respectively (Figure 2c and 3c). These emissions correspond to lower ^{1}CT singlet excited state energies compared to those in the Zeonex® matrix. The lowest triplet excited states were observed at 2.19

eV for **1-Mes** and 2.25 eV for **1-Tipp** in the CBP matrix (Figure 2c and 3c). Fluoride addition to these emitters caused further red shifts in the emission wavelengths, with **1-Mes+F** emitting at 649 nm and **1-Tipp+F** at 605 nm. The triplet excited state energies decreased to 1.75 eV for **1-Mes+F** and 1.88 eV for **1-Tipp+F** (Figure 2g and 3g). The singlet-triplet energy gaps for these fluoroborates were 0.16 eV (**1-Mes+F**) and 0.17 eV (**1-Tipp+F**). The lower singlet-triplet splitting resulted in more dominant TADF emission, along with a visible small RTP band at longer delay times (Figure 2g, 2h, 3g, 3h, and Table 1). However, there was also a significant reduction in the delayed emission contribution (DE/PF, Table 1), likely due to aggregation process. Calculations on **1-Mes** in a CBP matrix (ε=3.5, n_r=1.79) confirm a red shift in the fluorescence peak (Figure S5) of the relevant singlet state (S_2 in our calculations) to 2.87 eV (431 nm, k_f=1.8 ± 0.1×10^8 s^{-1}), but they underestimate the degree of red-shift due to insufficient participation of CT states in the ensemble. The phosphorescence peak, however, remains nearly unchanged at 1.99 eV (624 nm, k_p=1.7 ± 0.1×10^2 s^{-1}) due to the localized character of the triplet state (Figure S6). Calculations also indicate that rISC remains inaccessible for **1-Mes** in CBP due to the high average gap (> 0.3 eV). If the medium polarity is further increased (ε=7.0, n_r=1.4), rISC from T_1 to S_2 can outcompete phosphorescence (k_{rISC}=4 ± 3×10^3 s^{-1} *vs* k_p=6.3 ± 0.6×10^1 s^{-1}) due to more intense stabilization of S_2 states with CT character in the ensemble, making delayed fluorescence possible. Importantly, calculations account for dielectric effects but not solid-state ones, making comparisons with experimental results less straightforward.

Upon fluoride addition, calculations for **1-Mes-2F** predict a fluorescence peak at 1.72 eV (721 nm, Figure S5) and phosphorescence peak at 1.53 eV (808 nm, Figure S6), with rates of k_f=7.4 ± 0.8×10^6 s^{-1} and k_p=6 ± 3×10^3 s^{-1}. The red shift indicates the CT character of both S_1 and T_1 states.

Both ISC and rISC rates remain high (k_{ISC}=1.0 ± 0.1×10^8 s^{-1}, k_{rISC}=6 ± 4×10^8 s^{-1}) due to near-zero gaps.

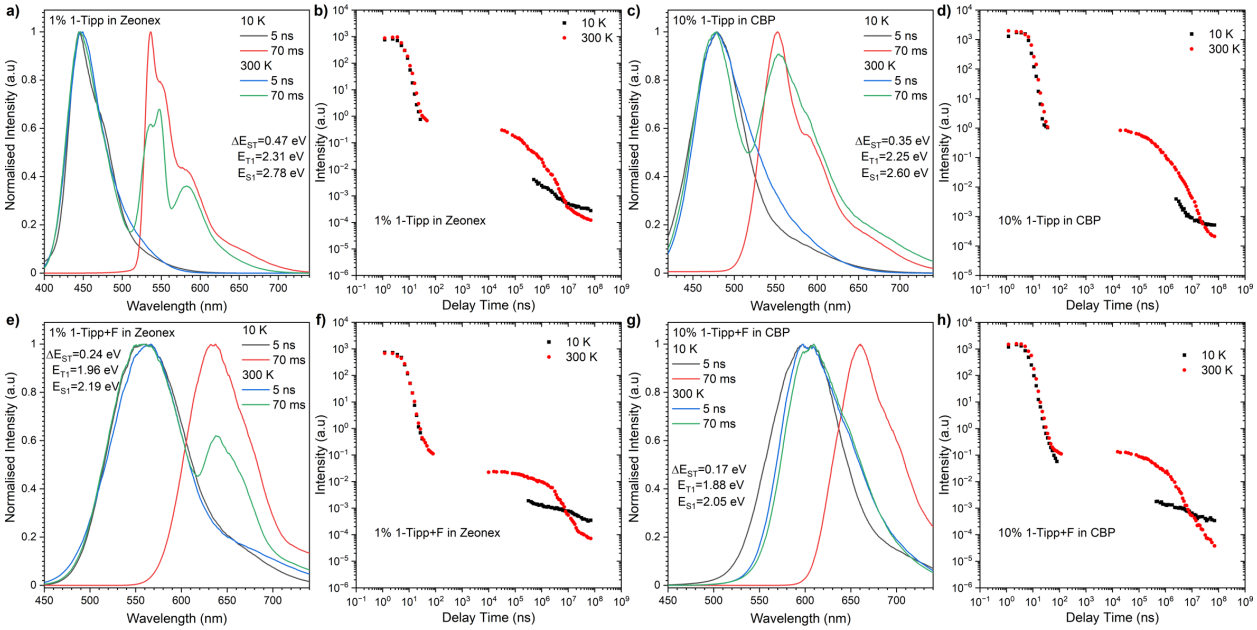

Figure 3. Time-resolved PL spectra (a, c, e, g) and decay profiles (intensity vs. delay time) (b, d, f, h) of **1-Tipp** and **1-Tipp+F** in Zeonex® and CBP. The energies correspond to the maximum emission peaks.

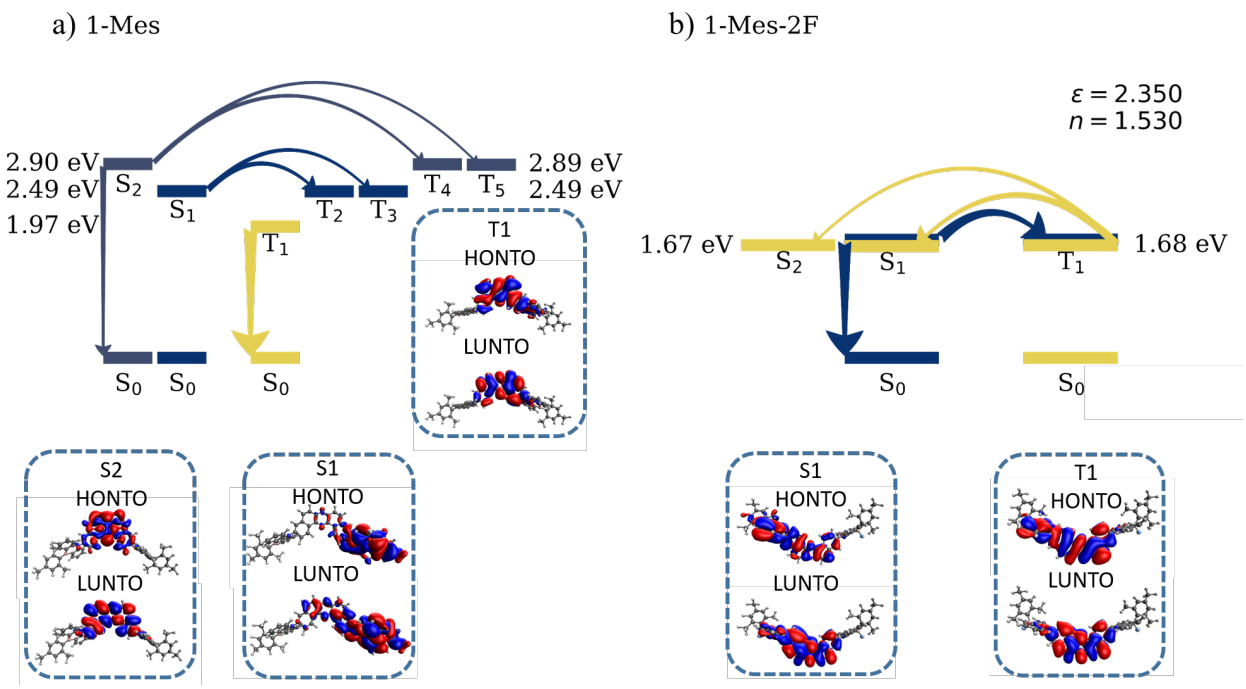

Figure 4. Energy level diagrams depicting the predicted photophysics of a) **1-Mes** and b) **1-Mes-2F** in Zeonex®. Natural transition orbitals (NTOs) of the most emissive geometries found in each molecule's ensembles are presented.

Delayed Emissions and Mechanisms

In the Zeonex® matrix, the neutral emitters **1-Mes** and **1-Tipp** exhibited substantial singlet-triplet energy gaps of 0.45 eV and 0.47 eV, respectively (Table 1), resulting in dual RTP and TTA delayed fluorescence emissions. TTA emission was observed at microsecond and millisecond delay timescales, with the rise of RTP at millisecond times indicating the presence of both TTA and RTP processes (Figure 2a and 3a). This resulted in significant DE/PF ratios of 2.0 and 3.4, respectively (Table 1). A kinetic model using rates computed from quantum chemical calculations predicts a biexponential decay with a prompt lifetime of 2.78 ns and a delayed lifetime of 5.76 ms, in agreement with the interpretation of prompt fluorescence followed by long-lived RTP (Figure S6). Emission on the microsecond timescale is not predicted, suggesting

that its experimental observation may be due to bimolecular phenomena not included in the model (Figure S7). Figure 4a illustrates the predicted photophysical mechanism for **1-Mes** in a Zeonex® film according to quantum chemical calculations.

In contrast, the fluorinated samples exhibited lower singlet-triplet energy gaps, resulting in TADF contributions rather than TTA, but still large enough to observe additional RTP emissions at millisecond delay times (Figure 2e and 3e). This behavior highlights the significant impact of formation of fluoroborate in reducing the singlet-triplet energy gap and activating the TADF process. Simulation results corroborate this, indicating two main emission components both stemming from fluorescence (Figure S8), signifying the TADF mechanism's contribution to the PL spectrum. However, simulated lifetimes are shorter than their experimental counterparts (0.8 ns and 0.14 μs), pointing to an overestimation of the ISC and rISC rates. These discrepancies can arise from inaccuracies in the electronic structure methods and unaccounted solid-state effects in the simulations. Figure 4b shows the photophysical mechanism of **1-Mes-2F** as predicted by quantum chemical calculations.

In the CBP matrix, the neutral emitters **1-Mes** and **1-Tipp** displayed lower singlet-triplet energy gaps compared to those in Zeonex®, leading to TADF emission. However, a RTP band was still observed at longer delay times in **1-Mes**, and mixed TTA/TADF and RTP emissions were seen for **1-Tipp** (Figure 2c and 3c). Fluorinated compounds **1-Mes+F** and **1-Tipp+F** in CBP showed further reduced singlet-triplet energy gaps, resulting in TADF emissions (Figure 2g and 3g), but also significant reductions in the DE/PF ratio (Table 1). Simulations performed for **1-Mes** in CBP show the same qualitative behavior as described for Zeonex® (Figures S9 and S10).

Table 1. Summary of the general photophysical properties obtained from time-resolved spectra.

Compound	λ_{em}, nm[a]	Host	PLQY %[b]	τ_{PF}, ns[c]	τ_{DF}, µs[d]	τ_{RTP}, ms[e]	DE/PF[f]	S_1 eV[g]	T_1, eV[g]	ΔE_{ST}, eV[h]
1-Mes	449	Zeonex	24.4	6.14 ± 0.27	70.53 ± 9.51	1.08 ± 0.18	2.00	2.76	2.31	0.45
1-Mes	504	CBP	28.7	6.59 ± 0.62	12.21 ± 2.00	-	6.64	2.46	2.19	0.27
1-Mes+F	596	Zeonex	9.2	5.31 ± 0.48	14.55 ± 1.05	-	0.24	2.08	1.87	0.21
1-Mes+F	649	CBP	8.4	8.15 ± 0.39	10.18 ± 1.23	-	0.95	1.91	1.75	0.16
1-Tipp	446	Zeonex	15.3	6.25 ± 0.53	141.14 ± 15.47	1.74 ± 0.12	3.34	2.78	2.31	0.47
1-Tipp	478	CBP	12.5	7.82 ± 0.66	292.21 ± 26.77	2.28 ± 0.23	4.60	2.59	2.25	0.35
1-Tipp+F	566	Zeonex	5.1	5.71 ± 0.47	219.57 ± 25.31	2.69 ± 0.17	1.22	2.19	1.96	0.24
1-Tipp+F	606	CBP	3.1	7.05 ± 0.66	180.81 ± 19.11	-	1.09	2.05	1.88	0.17

[a]The maximum wavelength of photoluminescence spectra; [b]Photoluminescence quantum yield in host under vacuum; [c]prompt fluorescence (PF) lifetime; [d]delayed fluorescence (DF) lifetime; [e]room temperature phosphorescence (RTP) lifetime; [f]ratio of delayed emission (DF & RTP) to prompt fluorescence (PF); [g]singlet and triplet energy (error ± 0.03 eV); [h]energy splitting (error ± 0.05 eV); All parameters estimated at 300 K.

The OLED devices were evaluated for their current density-voltage (J-V) characteristics, electroluminescence (EL) spectra, and external quantum efficiency (EQE) (Figure 5). The J-V measurements revealed non-linear current-voltage relationships, indicating efficient charge injection and transport. The EL spectra exhibited characteristic emission peaks corresponding to the TADF emitter and assistant dopant. Devices based on unfluorinated **1-Mes** (Sample A) achieved a maximum EQE of approximately 7.8%, while both fluorinated derivatives exhibited similar efficiencies around 2.3% (Figure 5c). The highest luminance was observed for the **1-**

Mes-based device (Sample A) at 15,000 cd/m². The EQE-luminance characteristics indicated an initial increase in EQE with increasing luminance, followed by a decrease at higher luminance levels due to competition between radiative and non-radiative recombination processes.

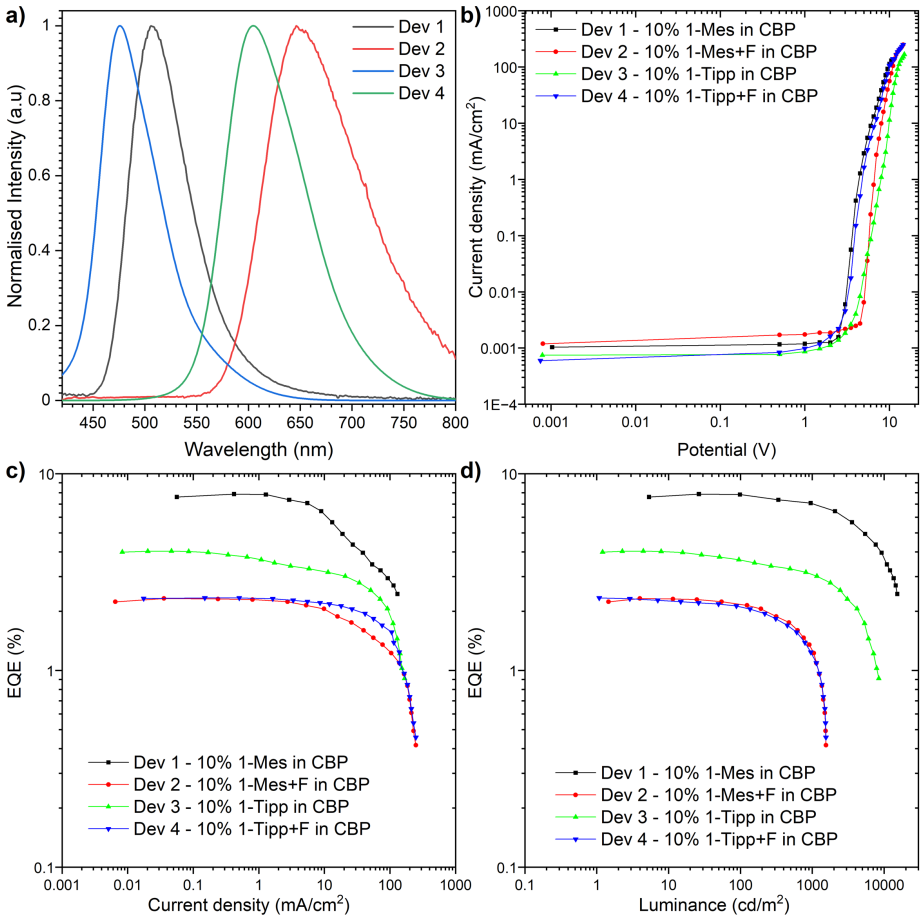

Figure 5. The characteristics of the OLED devices. Electroluminescence spectra (a). Current density-bias characteristic (b). EQE – current density (c). EQE - luminance characteristics (d).

CONCLUSIONS

The comparative analysis of TADF, TTA, and RTP highlights the diverse strategies available for enhancing OLED efficiency. TADF offers high efficiency through effective triplet harvesting,

TTA provides a simpler approach to utilizing triplets, and RTP enables unique emission properties. Tailoring organic emitters by optimizing molecular design, host-guest systems, and device architecture is crucial for advancing OLED technology and achieving highly efficient, stable, and versatile light-emitting devices. The findings from this study on phenazaborine-based compounds demonstrate the potential of strategic molecular modifications and host matrix selection in developing next-generation OLED materials. Fluorination of phenazaborine emitters signigicantly reduces the ΔE_{ST}, thereby, promoting TADF. However, the fabricated OLEDs with fluorinated emitters exhibited lower EQE compared to their non-fluorinated counterparts. This work identified potential efficiency bottlenecks, including Förster energy transfer, aggregation, and suboptimal device architecture. We have outlined promising pathways for improvement, such as developing non-doped devices, incorporating spacer groups, optimizing device architecture, exploring alternative materials, and employing computational modeling tools. By addressing these challenges, fluorinated phenazaborines hold immense potential for achieving high-performance TADF-OLEDs, paving the way for next-generation displays with superior efficiency.

ASSOCIATED CONTENT

Supporting Information. The Supporting Information is available free of charge at https://pubs.acs.org/doi/XXXX.

Experimental procedures for the spectroscopic analysis of materials, the preparation of organic light-emitting diodes and evaluation of their device performances (PDF)

Predicted photophysical data of the materials from theoretical calculations (PDF)

AUTHOR INFORMATION

Corresponding Author

*Piotr de Silva – Department of Energy Conversion and Storage, Technical University of Denmark, Anker Engelunds Vej 301, 2800 Kongens Lyngby, Denmark; Orcid: 0000-0002-4985-7350: E-mail: pdes@dtu.dk

*Przemyslaw Data – Department of Molecular Physics, Faculty of Chemistry, Lodz University of Technology, 90-543 Lodz, Poland; Orcid: 0000-0002-1831-971X: E-mail: przemyslaw.data@p.lodz.pl

*Youhei Takeda – Department of Applied Chemistry, Graduate School of Engineering, Osaka University, Suita, Osaka 565-0871, Japan; Orcid: 0000-0001-9103-4238; Email: takeda@chem.eng.osaka-u.ac.jp

Authors

Jaijanarthanan Lingagouder – Department of Molecular Physics, Faculty of Chemistry, Lodz University of Technology, 90-543 Lodz, Poland

Nae Aota – Department of Applied Chemistry, Graduate School of Engineering, Osaka University, Suita, Osaka 565-0871, Japan; Orcid: 0009-0006-7117-7411

Rikku Nakagawa – Department of Applied Chemistry, Graduate School of Engineering, Osaka University, Suita, Osaka 565-0871, Japan

Beata Luszczynska – Department of Molecular Physics, Faculty of Chemistry, Lodz University of Technology, 90-543 Lodz, Poland; Orcid: 0000-0002-4274-4222

Satoshi Minakata – Department of Applied Chemistry, Graduate School of Engineering, Osaka University, Suita, Osaka 565-0871, Japan; Orcid: 0000-0001-9619-445X
Leonardo Evaristo de Sousa: Department of Energy Conversion and Storage, Technical University of Denmark, Anker Engelunds Vej 301, 2800 Kongens Lyngby, Denmark; Orcid: 0000-0002-5880-5325

Author Contributions

The manuscript was written by Y.T. through contributions of all authors. All the experiences were conducted by J. L., N.O., and R.N. Quantum calculations were conducted by L.E.S. and P.S. All authors have given approval to the final version of the manuscript.

Notes

The authors declare no competing financial interest.

ACKNOWLEDGMENT

We acknowledge a Grant-in-Aid for Scientific Research on Innovative Area “Aquatic Functional Materials: Creation of New Materials Science for Environment-Friendly and Active Functions (Area No. 6104)” (JSPS KAKENHI Grant Number JP19H05716 for Y.T.) from the MEXT (Ministry of Education, Culture, Science and Technology, Japan), a Grant-in-Aid for Scientific Research (B) (JSPS KAKENHI Grant Number JP20H02813; JP23H02037 for Y.T.), a Grant-in-Aid for Challenging Research (Exploratory) (JSPS KAKENHI Grant Number JP21K18960 for Y.T.). P.deS. and L.E.deS. acknowledge a grant no. 2032-00144B from the

Independent Research Fund Denmark. Y.T. and S.M. acknowledge NIPPOH CHEMICALS for supplying *N,N*-diiodo-5,5-dimethylhydantoin (DIH). B.L. acknowledge support from the National Centre for Research and Development, Poland, Grant No. POLBER/5/63/PrintedQDD/2022. P.D. and J.L. acknowledges the Polish National Science Centre funding, grant no. 2022/45/B/ST5/03712.

REFERENCES

(1) Parker, C. A.; Hatchard, C. G. Triplet-Singlet Emission in Fluid Solutions. Phosphorescence of Eosin. *Trans. Faraday Soc.* **1961**, *57*, 1894–1904.

(2) Dias, F. B.; Penfold, T. J.; Monkman, A. P. Photophysics of Thermally Activated Delayed Fluorescence Molecules. *Methods Appl Fluoresc* **2017**, *5*, 012001.

(3) Chen, X.-K.; Kim, D.; Brédas, J.-L. Thermally Activated Delayed Fluorescence (TADF) Path toward Efficient Electroluminescence in Purely Organic Materials: Molecular Level Insight. *Acc. Chem. Res.* **2018**, *51*, 2215–2224.

(4) Uoyama, H.; Goushi, K.; Shizu, K.; Nomura, H.; Adachi, C. Highly Efficient Organic Light-Emitting Diodes from Delayed Fluorescence. *Nature* **2012**, *492*, 234–238.

(5) Nakanotani, H.; Tsuchiya, Y.; Adachi, C. Thermally-Activated Delayed Fluorescence for Light-Emitting Devices. *Chem. Lett.* **2021**, *50*, 938–948.

(6) Zhang, T.; Xiao, Y.; Wang, H.; Kong, S.; Huang, R.; Ka-Man Au, V.; Yu, T.; Huang, W. Highly Twisted Thermally Activated Delayed Fluorescence (TADF) Molecules and Their

Applications in Organic Light-Emitting Diodes (OLEDs). *Angew. Chem. Int. Ed.* **2023**, *62*, e202301896.

(7) Caine, J. R.; Hu, P.; Gogoulis, A. T.; Hudson, Z. M. Unlocking New Applications for Thermally Activated Delayed Fluorescence Using Polymer Nanoparticles. *Acc. Mater. Res.* **2023**, *4*, 879–891.

(8) Fang, F.; Zhu, L.; Li, M.; Song, Y.; Sun, M.; Zhao, D.; Zhang, J. Thermally Activated Delayed Fluorescence Material: An Emerging Class of Metal-Free Luminophores for Biomedical Applications. *Adv. Sci.* **2021**, *8*, e2102970.

(9) Ma, W.; Su, Y.; Zhang, Q.; Deng, C.; Pasquali, L.; Zhu, W.; Tian, Y.; Ran, P.; Chen, Z.; Yang, G. et al. Thermally Activated Delayed Fluorescence (TADF) Organic Molecules for Efficient X-Ray Scintillation and Imaging. *Nat. Mater.* **2022**, *21*, 210–216.

(10) Data, P.; Takeda, Y. Recent Advancements in and the Future of Organic Emitters: TADF- and RTP-Active Multifunctional Organic Materials. *Chem. Asian J.* **2019**, *14*, 1613–1636.

(11) Yamaguchi, S.; Wakamiya, A. Boron as a Key Component for New π-Electron Materials. *Pure Appl. Chem.* **2006**, *78*, 1413–1424.

(12) Berger, S. M.; Marder, T. B. Applications of Triarylborane Materials in Cell Imaging and Sensing of Bio-Relevant Molecules such as DNA, RNA, and Proteins. *Mater Horiz* **2022**, *9*, 112–120.

(13) Wade, C. R.; Broomsgrove, A. E. J.; Aldridge, S.; Gabbaï, F. P. Fluoride Ion Complexation and Sensing Using Organoboron Compounds. *Chem. Rev.* **2010**, *110*, 3958–3984.

(14) Yamaguchi, S.; Akiyama, S.; Tamao, K. Colorimetric Fluoride Ion Sensing by Boron-Containing π-Electron Systems. *J. Am. Chem. Soc.* **2001**, *123*, 11372–11375.

(15) Yamaguchi, S.; Shirasaka, T.; Akiyama, S.; Tamao, K. Dibenzoborole-Containing π-Electron Systems: Remarkable Fluorescence Change Based on the "On/off" Control of the p_π- π* Conjugation. *J. Am. Chem. Soc.* **2002**, *124*, 8816–8817.

(16) Liu, X. Y.; Bai, D. R.; Wang, S. Charge-Transfer Emission in Nonplanar Three-Coordinate Organoboron Compounds for Fluorescent Sensing of Fluoride. *Angew. Chem. Int. Ed.* **2006**, *45*, 5475–5478.

(17) Aota, N.; Nakagawa, R.; de Sousa, L. E.; Tohnai, N.; Minakata, S.; de Silva, P.; Takeda, Y. Anion-Responsive Colorimetric and Fluorometric Red-Shift in Triarylborane Derivatives: Dual Role of Phenazaborine as Lewis Acid and Electron Donor. *Angew. Chem. Int. Ed.* **2024**, *63*, e202405158.

(18) Takeda, Y.; Okazaki, M.; Minakata, S. Oxidative Skeletal Rearrangement of 1,1′-Binaphthalene-2,2′-Diamines (BINAMs) via C–C Bond Cleavage and Nitrogen Migration: A Versatile Synthesis of U-Shaped Azaacenes. *Chem. Commun.* **2014**, *50*, 10291–10294.

(19) Hirai, H.; Nakajima, K.; Nakatsuka, S.; Shiren, K.; Ni, J.; Nomura, S.; Ikuta, T.; Hatakeyama, T. One-Step Borylation of 1,3-Diaryloxybenzenes Towards Efficient

Materials for Organic Light-Emitting Diodes. *Angew. Chem. Int. Ed.* **2015**, *54*, 13581–13585.

(20) Hatakeyama, T.; Shiren, K.; Nakajima, K.; Nomura, S.; Nakatsuka, S.; Kinoshita, K.; Ni, J.; Ono, Y.; Ikuta, T. Ultrapure Blue Thermally Activated Delayed Fluorescence Molecules: Efficient HOMO-LUMO Separation by the Multiple Resonance Effect. *Adv. Mater.* **2016**, *28*, 2777–2781.

(21) Mamada, M.; Hayakawa, M.; Ochi, J.; Hatakeyama, T. Organoboron-Based Multiple-Resonance Emitters: Synthesis, Structure-Property Correlations, and Prospects. *Chem. Soc. Rev.* **2024**, *53*, 1624–1692.

(22) Data, P.; Pander, P.; Okazaki, M.; Takeda, Y.; Minakata, S.; Monkman, A. P. Dibenzo[*a,j*]phenazine-Cored Donor-Acceptor-Donor Compounds as Green-to-Red/NIR Thermally Activated Delayed Fluorescence Organic Light Emitters. *Angew. Chem. Int. Ed.* **2016**, *55*, 5739–5744.

(23) Okazaki, M.; Takeda, Y.; Data, P.; Pander, P.; Higginbotham, H.; Monkman, A. P.; Minakata, S. Thermally Activated Delayed Fluorescent Phenothiazine-Dibenzo[*a,j*]phenazine-Phenothiazine Triads Exhibiting Tricolor-Changing Mechanochromic Luminescence. *Chem. Sci.* **2017**, *8*, 2677–2686.

(24) Takeda, Y.; Kaihara, T.; Okazaki, M.; Higginbotham, H.; Data, P.; Tohnai, N.; Minakata, S. Conformationally-Flexible and Moderately Electron-Donating Units-Installed D-A-D Triad Enabling Multicolor-Changing Mechanochromic Luminescence, TADF and Room-Temperature Phosphorescence. *Chem. Commun.* **2018**, *54*, 6847–6850.

(25) Hirata, S.; Head-Gordon, M. Time-Dependent Density Functional Theory within the Tamm–Dancoff Approximation. *Chem. Phys. Lett.* **1999**, *314*, 291–299.

(26) Mewers, J.-M.; You, Z.-Q.; Wormit, M.; Kriesche, T.; Herbert J. M.; Dreuw, A. Experimental Benchmark Data and Systematic Evaluation of Two a *Posteriori*, Polarizable-Continuum Corrections for Vertical Excitation Energies in Solution. *J. Phys. Chem. A* **2015**, *119*, 5446–5464.

(27) de Sousa, L. E.; de Silva, P. Unified Framework for Photophysical Rate Calculations in TADF Molecules. *J. Chem. Theory Comput.* **2021**, *17*, 5816–5824.

(28) de Sousa, L. E.; de Silva, P. Photophysics of Solvated Molecules: Computational Protocol Combining Nuclear Ensemble and Nonequilibrium State-Specific Solvation Methods. *J. Phys. Chem. A* **2023**, *127*, 8200–8208.

(29) Shao, Y.; Gan, Z.; Epifanovsky, E.; Gilbert, A. T. B.; Wormit, M.; Kussmann, J.; Lange, A. W.; Behn, A.; Deng, J.; Feng, X. et al. Advances in Molecular Quantum Chemistry Contained in the Q-Chem 4 Program Package. *Mol. Phys.* **2014**, *113*, 184–215.

TOC Graphic

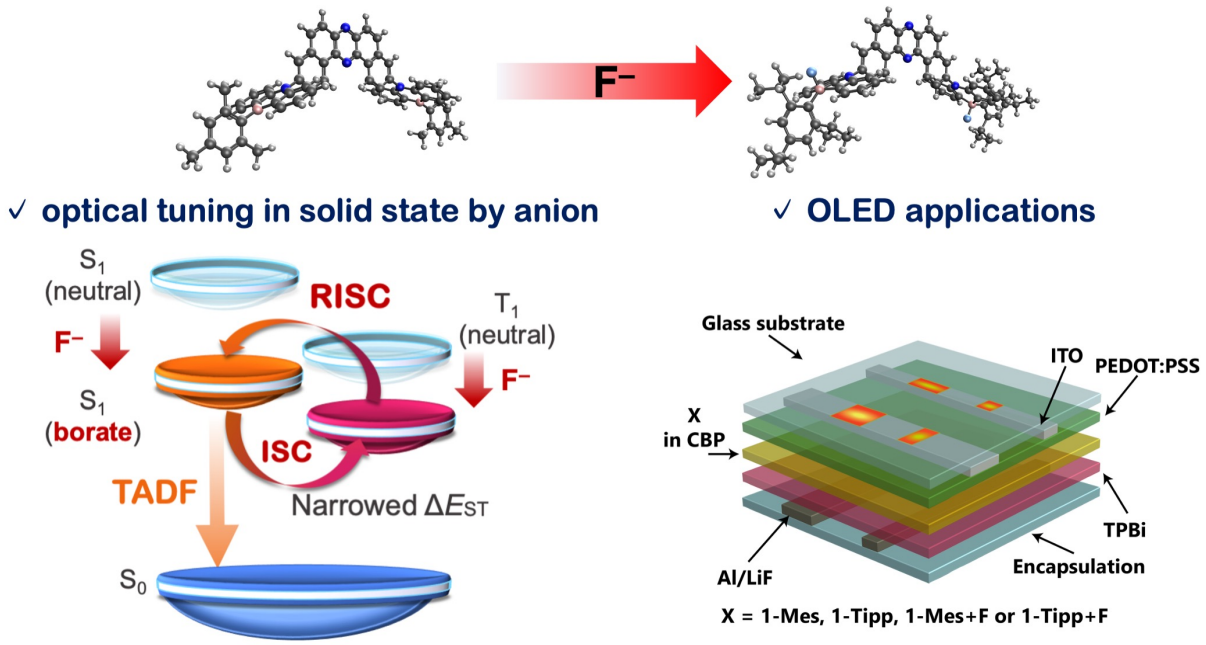
F⁻
✓ optical tuning in solid state by anion
✓ OLED applications
S1 (neutral)
F⁻
S1 (borate)
RISC
T1 (neutral)
F⁻
ISC
TADF
Narrowed ΔEST
S0
Glass substrate
ITO
PEDOT:PSS
X in CBP
TPBi
Al/LiF
Encapsulation
X = 1-Mes, 1-Tipp, 1-Mes+F or 1-Tipp+F